Rigorous Sensor Model of Gaofen-7 Satellite Laser Altimeter Based on Coupled Footprint Camera

Shaoning Li, Guo Zhang, *Member, IEEE*, and Xiufang Fan

***Abstract*—The Gaofen-7 (GF-7) satellite system adds a footprint camera that shares the same optical path as its laser altimeter to ensure consistent spatial referencing between the laser footprint point and the obtained optical images. However, this introduces additional errors between the two different loads while ensuring the geometric relations of the laser altimeter and footprint camera. First, the accuracy and error analyses of the laser altimeter and footprint camera are carried out based on the working mode of the GF-7 satellite laser altimeter and footprint camera in this study. A rigorous sensor model of laser geometric positioning is proposed based on the coupled footprint camera, which is achieved for the geometric correlation of laser spots on the ground and the focal plane of the footprint camera. The satellite laser altimeter simulation platform was used to analyze the various error sources in the geometric positioning of the laser altimeter, and GF-7 satellite data were used to verify the proposed geometric positioning model of the laser altimeter and footprint camera. The results show that the positioning error of the GF-7 footprint camera is less than 5 m (root-mean-square error) relative to the dual-line array image, which can provide ground control points for stereo mapping.**

***Index Terms*—Footprint camera, Gaofen-7 (GF-7), geometric calibration, laser altimeter satellite, rigorous sensor model (RSM).**

I. Introduction

SPACE-BORNE laser altimetry technology is an active remote sensing method for the accurate and rapid acquisition of surface elevation information. The distance between the altimeter and the measured target was obtained according to the time-of-flight of the pulse signal emitted by the laser altimeter [1], [2]. In 2003, the National Aeronautics and Space Administration obtained the laser data products derived from the Geoscience Laser Altimeter System (GLAS) instrument that flew on the Ice, Cloud, and land Elevation satellite (ICESat), demonstrating its unique advantages in the field of surface exploration [3], [4], [5], [6]. In 2018, the United States launched another ICESat-2 satellite, which carried a photon-counting laser altimeter system, the Advanced Topographic Laser Altimeter System [7], [8]. The laser altimeter system of the Global Ecosystem Dynamics Investigation was installed at the International Space Station in the same year, mainly for the detection of global surface three-dimensional (3-D) terrain and vegetation biomass [9], [10]. The use of space-borne laser altimetry technology began relatively late in China, and to promote its development, some experts have proposed carrying laser altimeters and stereo cameras on the same platform for stereo mapping [11], [12]. The altimetry system has been joined by the ZiYuan3-02 (ZY3-02) satellite launched in May 2016 and the ZiYuan3-03 (ZY3-03) satellite launched in July 2020. The successive launches of ZY3-02 and ZY3-03 satellites have confirmed the feasibility of a laser combined with a three-line array camera for stereo mapping [13], [14], [15], [16], [17], [18]. The Gaofen-7 (GF-7) satellite was launched in November 2019 and carries two laser altimeters with full waveform for global stereo mapping [19], [20], [21], [22], [23], [24], [25]. From the abovementioned research studies, the laser altimetry platform of Chinese satellite mainly adopts the large-spot measurement mode, which is combined with the optical camera on the same platform to obtain the data by a combination of active and passive remote sensing payloads.

Because traditional optical remote sensing images record the reflection intensity of surface features whereas laser altimeter data record the 3-D elevation of the surface, it is difficult for the two to achieve consistent spatial referencing by image matching. A footprint camera that images the ground utilizing the same optical path as the laser altimeter was introduced on the GF-7 satellite in order to construct a geometric registration of the laser footprint and optical images by recording the laser optical axis pointing. However, this process introduces error transfer between different measurement payloads. To achieve precise positioning of the laser footprint spot, researchers have constructed a rigorous geometric model of space-borne laser altimetry [3], [15], [16], but this model only transmits measurement parameters from the satellite platform, and the purpose of the laser footprint camera is neglected in the model. Based on the measurement and working mode of the GF-7 satellite's laser altimeter and footprint camera, this study analyzes the laser altimeter and footprint camera measurement error link transfer and accuracy. In order to achieve the geometric correlation of laser spots on the ground and the focal plane of the footprint

Manuscript received 11 June 2022; revised 1 September 2022, 13 October 2022, and 29 December 2022; accepted 1 February 2023. Date of publication 9 February 2023; date of current version 15 February 2023. This work was supported in part by the National Natural Science Foundation of China under Grant 41901400, in part by the project of the Scientific Research Fund of Hunan Provincial Education Department under Grant 20C0800, and in part by the project of the Natural Science Foundation of Hunan Province under Grant 2022JJ30254. *(Corresponding author: Guo Zhang.)*

Shaoning Li and Xiufang Fan are with the National-Local Joint Engineering Laboratory of Geo-Spatial Information Technology and the School of Earth Sciences and Spatial Information Engineering, Hunan University of Science and Technology, Xiangtan 411201, China (e-mail: lsn@hnust.edu.cn; fanxiufang@mail.hnust.edu.cn).

Guo Zhang is with the State Key Laboratory of Information Engineering in Surveying, Mapping and Remote Sensing, Wuhan University, Wuhan 430079, China (e-mail: guozhang@whu.edu.cn).

Digital Object Identifier 10.1109/JSTARS.2023.3242736

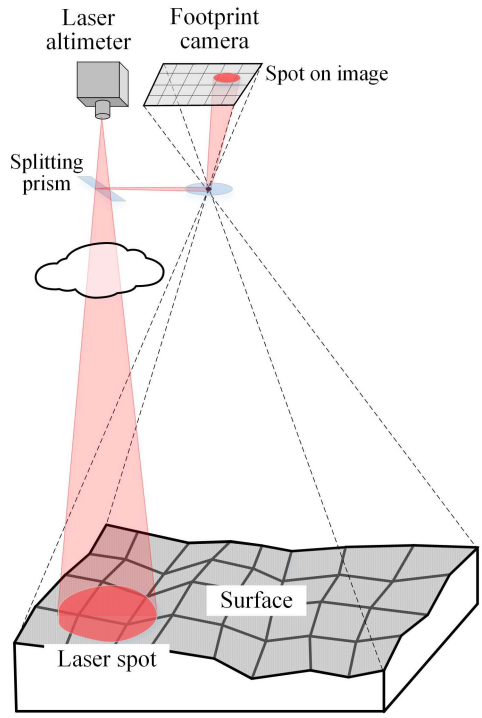

Fig. 1. Schematic of the laser altimeter and footprint camera measurement system.

camera, a rigorous sensor model (RSM) of the laser altimeter is constructed based on the coupled footprint camera.

II. GF-7 Laser Altimeter System

Because space-borne laser altimeter data are not used for imaging, it is difficult to record the environment at the observation location in real time, such as with optical cameras. To enhance the availability of laser altimeter data, a laser altimeter satellite platform was designed with an optical camera having the same optical path as the laser, namely the footprint camera. A footprint camera can record the position of the laser emission spot when imaging ground objects. The footprint camera is used to calculate the laser optical axis by recording the direction of the laser altimeter emission pulse rather than by directly imaging the ground laser spot. The geometric relationship between laser altimeter measurements and footprint camera imaging is shown in Fig. 1.

The pulse signal emitted by the GF-7 laser altimeter passes through a beam-splitting prism, part of the signal is transmitted into the imaging focal plane of the footprint camera, and the laser beam from the splitting prism is imaged on the footprint camera. The other part of the signal penetrates the atmosphere, clouds, aerosols, etc., to reach the ground and irradiate the light spot on the surface, which is called the "laser spot" shown in Fig. 1.

The footprint camera usually adopts a profiling array to record the laser spot, and there are two ways to identify the mode of laser emission pointing. The first is the mode adopted by the ICESat/GLAS satellite, which uses an electro-optical sensor

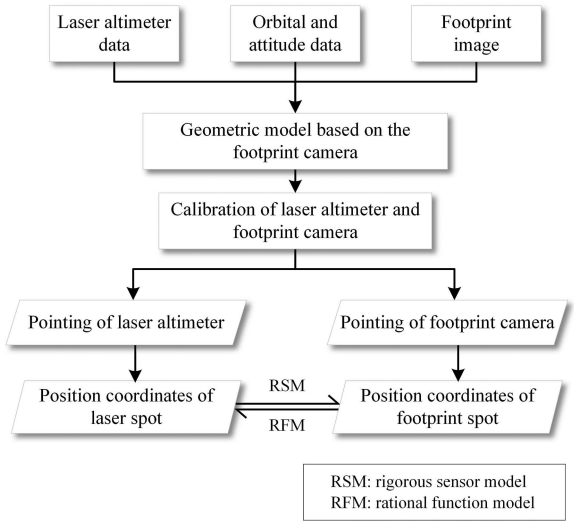

Fig. 2. Data processing of the laser altimeter and the footprint camera.

with charge-coupled device (CCD) array detectors to record a laser spot (40 Hz) with an array of 80×80 pixels. The laser beam is introduced into the star-sensitive camera to obtain the direction of the laser beam in the International Celestial Reference Frame. The other is that the GF-7 satellite uses a laser footprint camera to record the direction of the laser beam emission in the International Terrestrial Reference Frame, thereby determining the position of the laser spot on the ground image and its correlation with ground features. The GF-7 footprint camera implemented complementary metal–oxide–semiconductor (CMOS) array detectors to record a laser spot (3 Hz), and it mainly adopts the synchronous working mode, which means it records laser spot information while simultaneously imaging surface features.

III. Methodology

Fig. 2 shows the data processing techniques according to the working mode of the GF-7 satellite laser altimeter and footprint camera.

A. Rigorous Sensor Model

The coordinate system of the laser altimeter and footprint camera is constructed, as shown in Fig. 3. The satellite body coordinate system is known as O-XYZ, which is used to describe each sensor's position and the orientation of the optical axis with respect to the coordinate frame. The laser altimeter coordinate system O_{Las}-$X_{Las}Y_{Las}Z_{Las}$ is defined as follows: The pointing of the three axes is consistent with the body coordinate system, the origin of the coordinate system O_{Las} is located at the laser pulse emission point, and the optical axis center of the laser altimeter points to (φ_L,ω_L). The focal plane of the footprint camera is a planar right-angle coordinate system that describes the arrangement of CMOS probe elements in the focal plane. The footprint camera coordinate system O_F-$X_FY_FZ_F$ is defined as follows: The origin of the coordinate system O_F is located at the center of the optical lens, the Z_F axis is the main optical

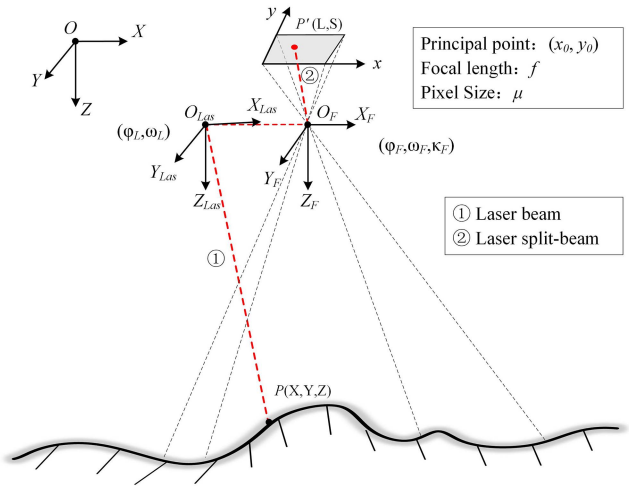

Fig. 3. Coordinate system of the laser altimeter and the footprint camera.

axis direction of the camera, perpendicular to the focal plane and pointing to the ground direction, the X_F axis is parallel to the *x*-axis of the focal plane, the Y_F axis is parallel to the *y*-axis of the focal plane, and the installation angles of the footprint camera relative to the body coordinate system is (φ_F, ω_F, κ_F).

The spot of light where a laser beam illuminates on the ground can be obtained by the detectors in the calibration field. The actual pointing of the laser beam can be determined with respect to the laser altimeter frame by on-orbit calibration. Meanwhile, another spot of light splitting from the same laser beam is caught on the footprint camera of the GF-7 satellite, and the pointing of the split beam can be determined with respect to the footprint camera frame by centroid extraction. Then, the geometric relationship between the optical axis of the laser beam and the laser split-beam is constructed by the coordinate system of the laser altimeter and its coupled footprint camera. But the two laser beams are not usually parallel, and there is a slight angular deviation between the laser emitting beam and the splitting beam in order for the footprint camera to record the ground objects around the actual spot on the ground. Thus, it can be seen that the imaged spot will not be the same as the actual footprint on the ground plane. In order to determine the slight angular deviation between the two laser beams, the laser altimeter and footprint camera need to be calibrated at the same time and in the same field. Here, the data processing flow of on-orbit calibration for the GF-7 satellite laser altimeter and the footprint camera is shown in Fig. 4.

The error transfer term of the laser measurement link mainly involves errors in on-orbit calibration, footprint camera installation measurement, spot center extraction, etc. Thus, the laser geometric positioning model based on the footprint camera is constructed in accordance with the following equation:

$$P\ (X,Y,Z) = (O_{\text{Las}})_{\text{WGS84}} + L \cdot R\,(t) \cdot R\,(\text{Las}) \cdot R\,(F) \cdot U\,(L,S) \tag{1}$$

where $P(X,Y,Z)$ are the coordinates of the laser footprint center on the ground; $(O_{\text{Las}})_{\text{WGS84}}$ is the position coordinate of the laser emitting point in the WGS84 coordinate system; L is the laser range value; $R(t)$ is the conversion matrix between the body coordinate system and the satellite attitude measurement coordinate system; $R(\text{Las})$ is the conversion matrix between the laser altimeter calibration coordinate system and the defined coordinate system; $R(F)$ is the installation matrix of the laser footprint camera under the satellite platform; and $U(L,S)$ is the point of the laser split-beam optical axis in the footprint camera coordinate system.

B. Geometric Calibration

The GF-7 laser altimeter and footprint camera are calibrated at the same time and in the same field [23], [24]. The real-time laser signals are obtained from the satellite by laying out detector arrays on the ground. Four optical targets around the laser detector arrays are used to collect ground control points (GCPs) for calibrating the footprint camera simultaneously. Then, we can get the precise optical axes of the laser altimeter and footprint camera, as shown in Fig. 5.

In the data processing of on-orbit geometric calibration, the energy distribution of the laser footprint is obtained from the detector arrays on the ground. A Gaussian fitting method is used to find the center of the laser footprint spot. Then we can calculate the pointing of the satellite laser beam combining with satellite position. There is a great deal of uncertainty between the actual optical axis pointing and the optical axis pointing before launch. To optimize the efficiency of laser altimeter calibration, a calibration field on flat terrain where the laser beam is hitting has to be selected according to the precise position of the satellite and a rough pointing of the laser beam [14], [16].

A pointing matrix and a ranging deviation parameter are adopted in the laser geometric model for compensation of ranging and pointing errors. The calibration model of the laser spot's geographical location is deduced as follows:

$$P\ (X,Y,Z) = (O_{\text{Las}})_{\text{WGS84}} + (L+dL) \cdot R\,(d\varphi, d\omega, 0) \cdot R\,(t) \cdot \begin{bmatrix} \cos(\varphi_L)\sin(\omega_L) \\ \cos(\varphi_L)\cos(\omega_L) \\ \sin(\varphi_L) \end{bmatrix}. \tag{2}$$

where $(O_{\text{Las}})_{\text{WGS84}}$ is the position of the laser emitting point on the satellite; L is the value of laser ranging; dL is the ranging deviation parameter of the laser altimeter based on the calibration; $d\varphi$ and $d\omega$ are the pointing calibration parameters for the laser on-orbit calibration; $R(t)$is the attitude matrix to record the attitude state of the satellite platform; and $\begin{bmatrix} \cos(\varphi_L)\sin(\omega_L) \\ \cos(\varphi_L)\cos(\omega_L) \\ \sin(\varphi_L) \end{bmatrix}$ is the pointing of the laser beam with respect to the laser altimeter coordinate frame. The calibration parameters dL, $d\varphi$, and $d\omega$ can be calculated if the geographic coordinates $P(X,Y,Z)$ of the laser footprint spot on the ground are obtained from the detector arrays in the calibration field.

C. Pointing of Laser Beam

The optical axis pointing of the laser split-beam was obtained using the spot-on image of the footprint camera. The traditional

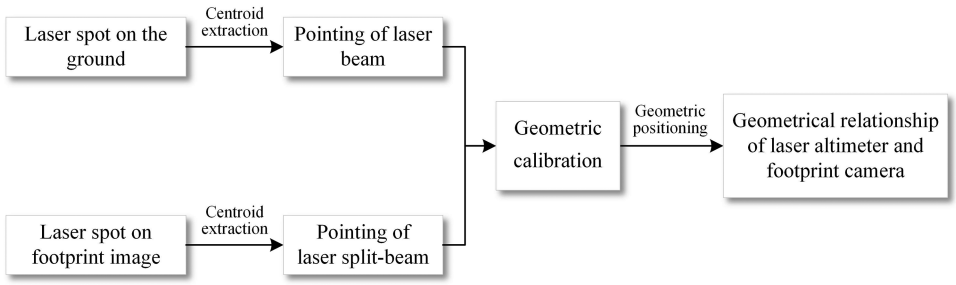

Fig. 4. On-orbit calibration processing of the laser altimeter and the footprint camera.

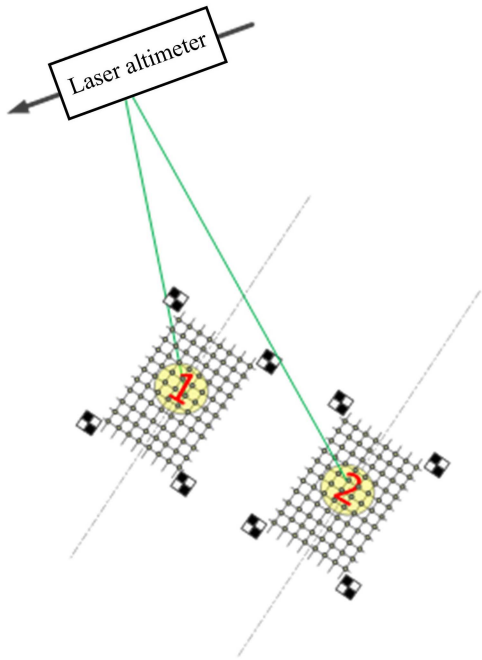

Fig. 5. Calibration of the laser altimeter and the footprint camera.

center extraction methods of a laser spot include the Gaussian fitting algorithm, the ellipse fitting algorithm, the intensity centroid method, etc. [25], [26]. The accuracy of the laser spot's center will be greatly affected by the strong reflection intensity of ground objects on the footprint camera image. To improve the extraction accuracy of the footprint spot's center, a Gaussian fitting method based on intensity weighting to solve the position of the footprint spot's center is used in this study. Assuming that the size of the footprint spot image is $M \times N$ pixels and the intensity value of each pixel is $I_0(i,j)$, the initial center position (L_0, S_0) of the footprint spot is first solved using the traditional intensity centroid method, as shown in the following equation:

$$\begin{cases} L_0 = \sum_{i=1}^{M}\sum_{j=1}^{N} i \cdot I_0(i,j) \,/\, \sum_{i=1}^{M}\sum_{j=1}^{N} I_0(i,j) \\ S_0 = \sum_{i=1}^{M}\sum_{j=1}^{N} j \cdot I_0(i,j) \,/\, \sum_{i=1}^{M}\sum_{j=1}^{N} I_0(i,j) \end{cases}. \tag{3}$$

The intensity value of the spot image is then recalculated by distance weighting using the Gaussian function, and the Euclidean distance d from the pixel intensity value $I_0(i,j)$ to the initial center position (L_0, S_0) is used as the weight value to calculate the intensity value $I(i,j)$ of the new spot image, as in the following equation:

$$\begin{cases} G\ (d) = \mathrm{e}^{-\left(\frac{d}{\sigma}\right)^2} \\ I\ (i,j) = G(d) \cdot I_0(i,j) \end{cases}. \tag{4}$$

Next, the center of the spot (L, S) was obtained by Gaussian fitting to the new footprint spot image as follows:

$$I\ (i,j) = A \cdot \exp\left[-\frac{(i-L)^2}{2\sigma_1^2} - \frac{(j-S)^2}{2\sigma_2^2}\right]. \tag{5}$$

where A is the amplitude value of the footprint spot, and σ_1 and σ_2 are the standard deviations of the footprint image's line and sample, respectively.

Using the geometrical parameters of the footprint camera, the pointing of the laser split-beam optical axis can be solved as follows:

$$\begin{cases} U(L) = arctan(L \cdot \mu / f) \\ U(S) = arctan(S \cdot \mu / f) \end{cases} \tag{6}$$

where μ denotes the probe element size in the focal plane of the footprint camera and f is the focal length of the footprint camera imaging.

D. Geometric Positioning

There is a slight deviation in the plane if the position coordinates of the laser footprint center on the ground are projected directly on the footprint image. The positioning model of the laser beam mentioned above is used to establish the correlation between the laser spot's center on the ground and the spot's center on the footprint camera image, and then the image coordinates (L', S') of the laser spot's center on the ground are solved using the position (L, S) of the image, as shown in the following equation:

$$\begin{aligned} (L', S') = U^{-1}\ \big[&R^{-1}(\varphi_F, \omega_F, \kappa_F) \cdot R(d\varphi, d\omega, 0) \\ &\cdot R(\varphi_F, \omega_F, \kappa_F) \cdot U(L, S)\big]. \end{aligned} \tag{7}$$

A rational function model is used to locate the optical image rather than the rigorous imaging model on normal. The geographic coordinates of the ground point and its corresponding image point coordinates are fitted with a ratio polynomial, as

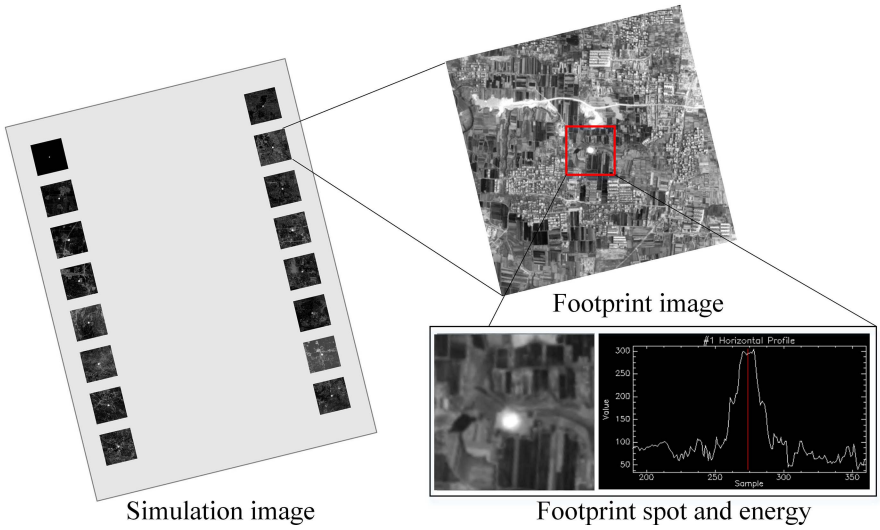

Fig. 6. Simulation images of the footprint camera.

shown in the following equation:

$$\begin{cases} x = \frac{f_1(lat,lon,H)}{f_2(lat,lon,H)} \\ y = \frac{f_3(lat,lon,H)}{f_4(lat,lon,H)} \end{cases} . \tag{8}$$

where x and y are the pixel coordinates of the footprint image; $f_i(lat, lon, H)$ ($i = 1$, 2, 3, and 4) is a polynomial function of the geographic coordinates *lat*, *lon,* and *H* of the laser footprint, where the polynomial coefficients are given as follows:

$$f_i\ (lat, lon, H) = \sum_{i=0}^{3}\sum_{j=0}^{3}\sum_{k=0}^{3} a_{ijk} lat^i lon^j H^k . \tag{9}$$

The coordinates of the laser spot's center on the ground can then be calculated using the rational function model, and the inverse form of the rational function model, by which the laser spot's center on the image is established in a geometric relationship to the laser spot's center on the ground, can be obtained according to (8), expressed as follows:

$$\begin{cases} lat = \frac{f_5(x,y,H)}{f_6(x,y,H)} \\ lon = \frac{f_7(x,y,H)}{f_8(x,y,H)} \end{cases} \tag{10}$$

where $f_i(x, y, H)$ ($i = 5$, 6, 7, and 8) can be used as a cubic polynomial with respect to x, y, and H, as described in (9).

IV. Experiment and Analysis

In this study, the RSM validation of the satellite laser altimeter based on the footprint camera was performed using simulated data and GF-7 satellite laser altimeter data. The simulation experiments were carried out to distinguish the effects of various types of errors, including the optical axis of the laser beam, laser spot's center on the calibration field, and the positioning of footprint spot. The experiments of the GF-7 satellite laser altimeter at Qingdao and Tianjin were used to verify the positioning accuracy of the laser spot relative to the stereo camera.

TABLE I
Simulation Parameters of the GF-7 Laser Altimeter System

Parameter item	Simulation parameter
Orbital altitude	505 km
Laser emission frequency	3 Hz
Energy of pulse	100 mJ
Pulse width	5–7 ns
Shape of laser waveform	Gaussian distribution
Resolution of footprint camera	3.2 m
Diameter of footprint spot	15–20 m

A. Simulation Experiment and Analysis

1) Simulation Data: The high-resolution airborne data in Songshan, China implemented by airborne photography were employed in the simulation experiment, including the orthoimage and digital elevation model. According to the design parameters of the GF-7 satellite laser altimeter (as shown in Table I), a satellite image was simulated in an area of 20 km × 20 km experimentally, and the resolution of the simulated image was consistent with the GF-7 satellite images. A pair of laser altimeters were simulated to obtain the laser waveforms and footprint camera images, and a total of 16 laser pulses were emitted in the area within the satellite image area, as shown in Fig. 6.

The simulation software integrated satellite and laser altimeter data processing were constructed according to the design of the GF-7 satellite. The error parameter terms of satellite and laser altimeter are listed in Table II.

The measurement error of the satellite platform included the orbit and attitude measurement errors. In the data processing,

TABLE II
ERROR PARAMETERS OF THE SATELLITE PLATFORM AND LASER ALTIMETER

Parameter item	Value
Orbit measurement error	0.05 m
Attitude measurement error	1.0 inch
Ranging error	0.5 ns
Noise rate of laser emission signal	5.0 %
Noise rate of laser detector	7.8 %
Noise rate of footprint spot	5.0 %

precise orbit determination (POD) of the GF-7 satellite was adopted to calculate the position of the laser spot on the ground. The measurement error of POD was less than 0.05 m (1σ), and a random function was adopted for the orbit measurement error in the simulation processing. The ranging error is mainly due to the waveform decomposition and the random error of the instruments' measurement. The maximum measurement error of laser ranging is no more than 0.5 ns in the calibration field for the echo waveform with only a single peak. All the random errors of the satellite platform and laser altimeter are at normal distribution. The attitude simulation data of the satellite platform were then simulated with errors based on the orbital position and velocity and combined with the attitude stability of the satellite platform. From the laser positioning model, it was observed that the platform attitudes affecting the positioning of the laser footprint points were mainly the roll and pitch angles, whereas the positioning error caused by the yaw angle was negligible.

2) Calibration and Precision Analysis: The most effective method of obtaining control data for on-orbit calibration is to deploy laser detectors on the ground to obtain the precise positions and energy distributions of laser footprint spots. The accuracy of the laser spot position obtained by the ground detector is mainly due to the interval and consistency of the laser detectors. To optimize the efficiency and performance of the laser detectors, the calibration processing of the satellite laser altimeter is simulated to determine the accuracy of the laser footprint spot's control data, and it can provide a reference for geometric calibration of the GF-7 satellite laser altimeter.

To validate the simulated calibration processing, a set of laser footprint images was collected in the laboratory. The laser spot's energy distribution obtained from the laser footprint images was used as a benchmark. Assuming that the diameter of the laser footprint spot on the ground is 15–20 m, the sampling value of laser detectors was performed according to laser footprint images, and the consistency ratio of the detectors is adjusted by increasing the random error to the sampling value. Thereafter, 10 000 sets of laser spots on the ground obtained by the detectors were simulated under each set of variable conditions (different intervals and different consistency ratios of detectors). Then, the position of each spot's center is calculated and counted, with the interval of the laser detector on the calibration field set between 1 and 15 m, and the results are shown in Fig. 7.

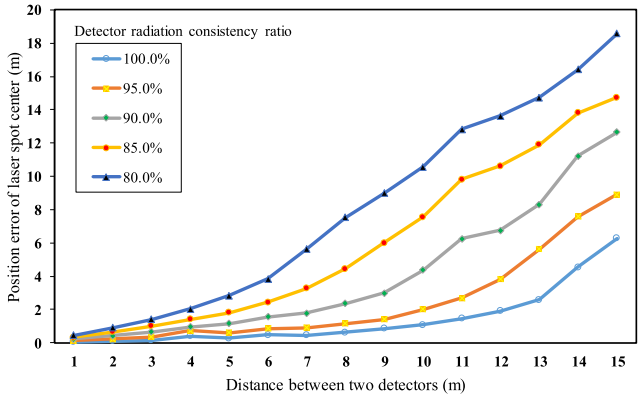

Fig. 7. Calibration error of the laser footprint spot.

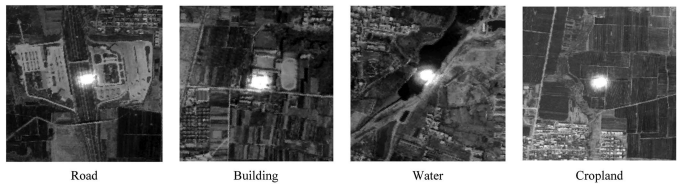

Fig. 8. Simulation images of the footprint camera.

It can be concluded from the simulation experiment results that the farther the distance between the adjacent detectors, the worse the extraction accuracy of the footprint spot's center. Besides, the extraction accuracy of the footprint spot's center is also limited by the consistency of the detectors. Due to the impacts of the detector errors, such as the factory calibration of the detector, the detector attitude, and dust pollution on the sensor during the calibration, it is difficult to ensure the consistency ratio of the satellite signal received by the detector. Therefore, to improve the geometric accuracy of the laser optical axis, the interval between adjacent detectors should be as dense as possible, considering the cost of the calibration experiment. In order to ensure that the pointing accuracy of the laser optical axis is no more than 1.0 s (positioning accuracy of the spot's center is no more than 2.4 m), it is needed to make sure that the consistency ratio of the detectors is not less than 90% and the distance between two adjacent detectors is no more than 8.0 m. The result of this simulation experiment will support the calibration of the GF-7 satellite laser altimeter.

3) Positioning and Precision Analysis: There is a random deviation in the pointing of the laser beam if the laser altimeter emits the pulse signal. The footprint camera can be used to establish the geometric correlation between the imaging of the ground objects and the position of the laser footprint spot. In this experiment, we simulated the laser spot on the footprint camera images (see Fig. 8). The areas imaged by the footprint camera contain roads, buildings, water, cropland, and other objects.

The simulated footprint images were processed to obtain the positions of the footprint spot's center from the two laser altimeters. A total of 16 laser spots were compared with the simulated reference values to analyze the distribution of position

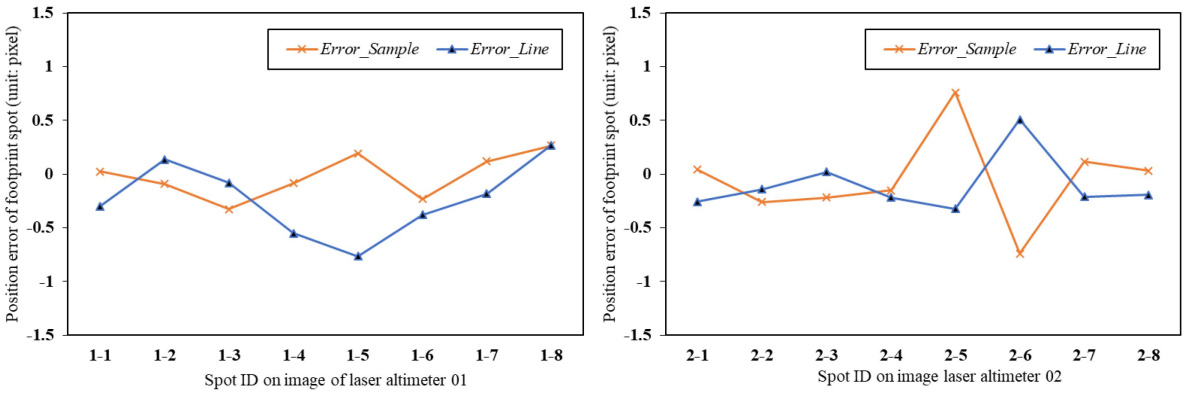

Fig. 9. Laser spot center errors of the synchronous footprint camera.

TABLE III
LASER FOOTPRINT POSITIONING ERROR (M)

Laser	Points	Positioning error						
		RMS			Maximum		Minimum	
		X	Y	XY	X	Y	X	Y
Laser_01	8	3.578	1.625	3.929	3.267	1.642	–6.347	–3.001
Laser_02	8	2.639	2.759	3.818	5.391	1.458	–3.335	–4.884
Total	16	3.144	2.264	3.874	5.391	1.642	–6.347	–4.884

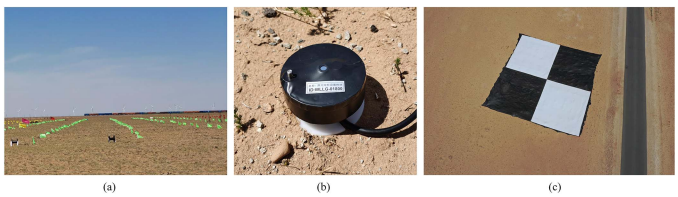

Fig. 10. Calibration field of the GF-7 satellite. (a) Calibration field. (b) Laser detector. (c) Optical target.

error for the laser footprint cameras, as shown in Fig. 9. The maximum spot-center extraction error in the footprint image was +0.762 pixels, and the minimum error was −0.732 pixels. The average values of the center position rank error were −0.034 pixels and −0.165 pixels, and the mean square errors (MSEs) were 0.314 pixels and 0.338 pixels, respectively. If the laser beam hits a strongly reflecting surface, such as a building, the intensity value around the spot on the footprint image is close to saturation, resulting in a large error in the extraction of the spot center position.

In this study, the accuracy of the laser geometric positioning model based on the footprint camera was analyzed using a link simulation of star–ground integration. The position of the laser footprint spot was determined by the geometric positioning model of the laser altimeter, and the positioning error results of the laser beams were obtained as shown in Table III.

From the simulation results, it can be seen that the relative pointing deviation between the laser optical axis and the optical axis of the footprint camera is approximately 1.5 in after the geometric calibration. The MSE of the plane positioning of the laser spot can reach within 4.0 m. The results of the current study show that the positioning accuracy of the satellite laser spots on the calibration fields is better than 5.0 m, and the vertical accuracy of the laser altimeter can reach 0.10 m [20], [25]. According to the simulation conditions, the laser spot positioning error caused by the orbit and attitude measurement errors of the satellite platform is approximately 2.0–3.0 m. The positioning accuracy of the GCPs on the GF-7 calibration field can reach approximately 4.0 m. This positioning accuracy is essentially consistent with the simulation results of this study. The simulation result also proves that the geometric positioning model for the laser altimeter and footprint camera is feasible in this study. The positioning accuracy of the footprint spot's center mainly depends on the attitude and orbit measurement of the satellite platform, geometric calibration, and spot center extraction. The subsequent validation experiments were conducted using the laser spots, footprint images, and stereo images of the GF-7 satellite.

B. *Experiment of the GF-7 Laser Altimeter*

The GF-7 satellite was launched on November 3, 2019, and the main payloads on the satellite are a dual-linear array camera

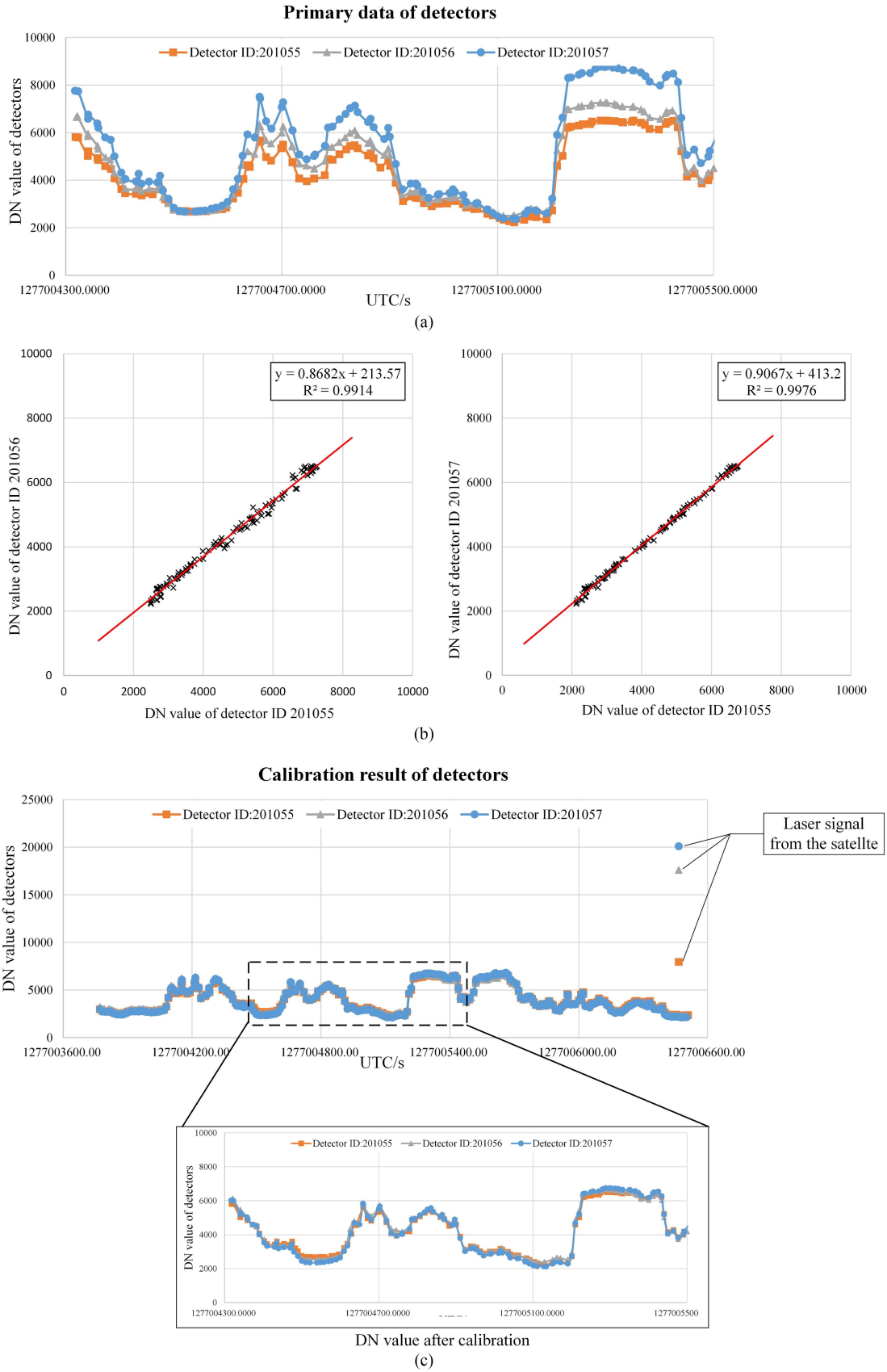

Fig. 11. Calibration results of laser calibration detectors. (a) Primary data obtained from detectors. (b) Linear regression analysis of detectors. (c) Calibration of radiation consistency.

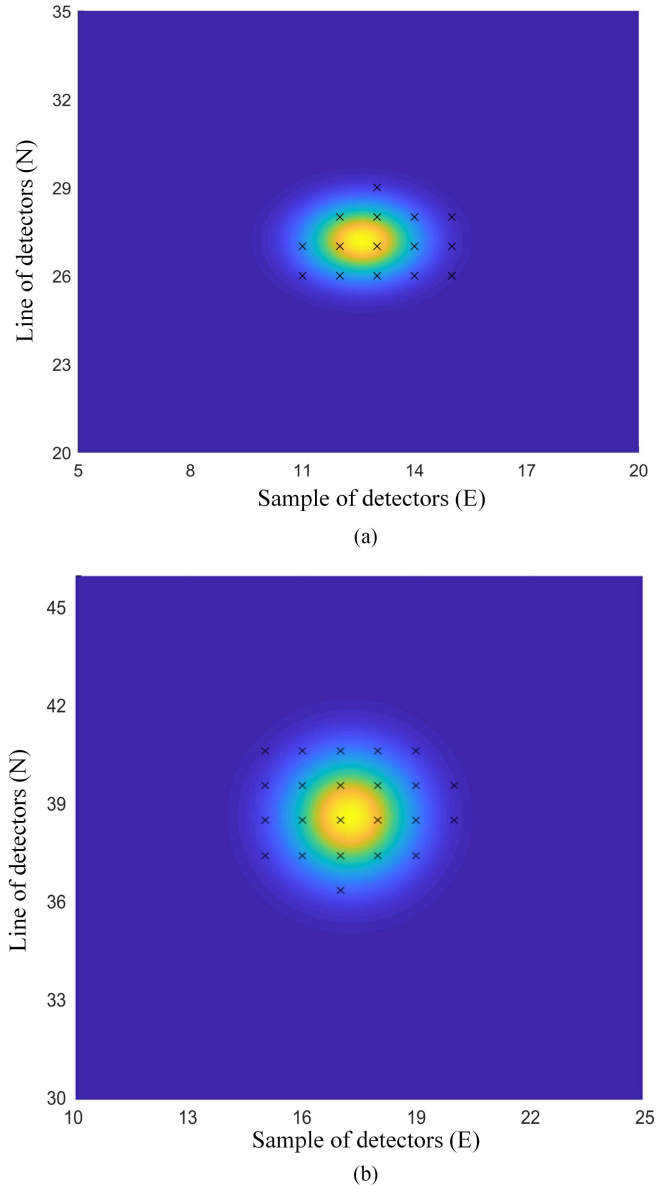

Fig. 12. Fitting results of laser calibration detectors. (a) Laser altimeter 01. (b) Laser altimeter 02.

and a pair of laser altimeters to acquire high-spatial-resolution optical stereo images and laser waveforms. In June 2020, the Land Satellite Remote Sensing Application Centre of China conducted calibration experiments of the GF-7 satellite laser altimeter in Inner Mongolia.

1) Calibration of Laser Altimeters: After predicting the positions of the laser footprint spots on the ground, an appropriate field near the center of the predicted spot was selected where the detectors were installed. The length (along the direction of the orbit) and width (vertical the direction of the orbit) of each calibration field were approximately 400 m $\times$ 150 m, and the interval of adjacent detectors was set between approximately 5.0 and 8.0 m. Four optical targets were set in the four corners of the laser calibration field, and the geometric parameters of the footprint camera were calibrated simultaneously. The calibration field, laser detectors, and optical targets of the GF-7 satellite are shown in Fig. 10. The calibration field is a flat area in the Gobi Desert without any vegetation.

It is difficult to ensure that the laser detectors are pointing directly at the satellite when a large number of detectors are set up in the calibration field. The consistency ratio of the detector terminal also varies, resulting in inconsistencies in the intensity of the laser signals obtained by the detectors. The inconsistencies will directly affect the extraction accuracy of the laser footprint spot's center. The effective signal threshold of the detector was adjusted downward during the experiment, and it can record the changes in the intensity of solar radiation in real time. The primary signal of the three detectors is shown in Fig. 11(a).

We can see that the changes in the solar radiation intensity will cause fluctuations in the signal intensity recorded by the detectors in Fig. 11(a). Assuming that the intensity of the solar radiation irradiating the detectors at the same time is consistent, the relative consistency ratio of each detector can be checked.

Within the effective signal acquisition range of the detectors, the signal intensity of different detectors varies linearly, and the consistency check model was obtained using the linear regression model, as shown in the following equation:

$$y = A_0 \cdot y_0 + K. \tag{11}$$

where y_0 is the signal intensity of the reference detector, A_0 is the primary coefficient of linear correlation, and K is the coefficient of the constant term. Here, the detector of No. 201055 was used as the reference benchmark. Then, the coefficients of different detectors are obtained, and the linear regression analysis of detectors is shown in Fig. 11(b). The detectors are checked for the relative consistency ratio between the different detectors, and the results are shown in Fig. 11(c).

First of all, the false trigger signals from the detectors are eliminated in the data processing of the laser altimeter calibration. To ensure that the relative consistency ratio of the detectors is not less than 90%, the valid signals from the detectors are screened. The position coordinates of the laser footprint spot's center are obtained by Gaussian fitting, as shown in Fig. 12. The geometric calibration parameters of satellite laser altimetry can be solved using the laser spot center coordinates as control points.

The main way to get the GCPs for the satellite laser altimeter is from the detectors on the calibration fields. The amount of GCPs required to verify the measurement accuracy of a satellite laser altimeter is very small. As it is difficult to separate the measurement error of the satellite platform from the positioning error of the laser spot, most of the GCPs from the laser detectors on the calibration fields are used to calculate the optical axis of the laser altimeter with respect to the satellite coordinate frame. To verify the positioning accuracy and stability of the laser altimeter, the coupled footprint camera is used to determine the geometric relationship between the optical axis of the laser altimeter and the dual-linear array cameras. The geometric parameters of the optical axis between the footprint camera and laser altimeter after calibration concurrently are invariant in a very long orbital period. The accuracy of the footprint camera can reach within 0.2 pixels after the geometric calibration using the optical targets [27], [28]. The positioning accuracy of the laser spot can be

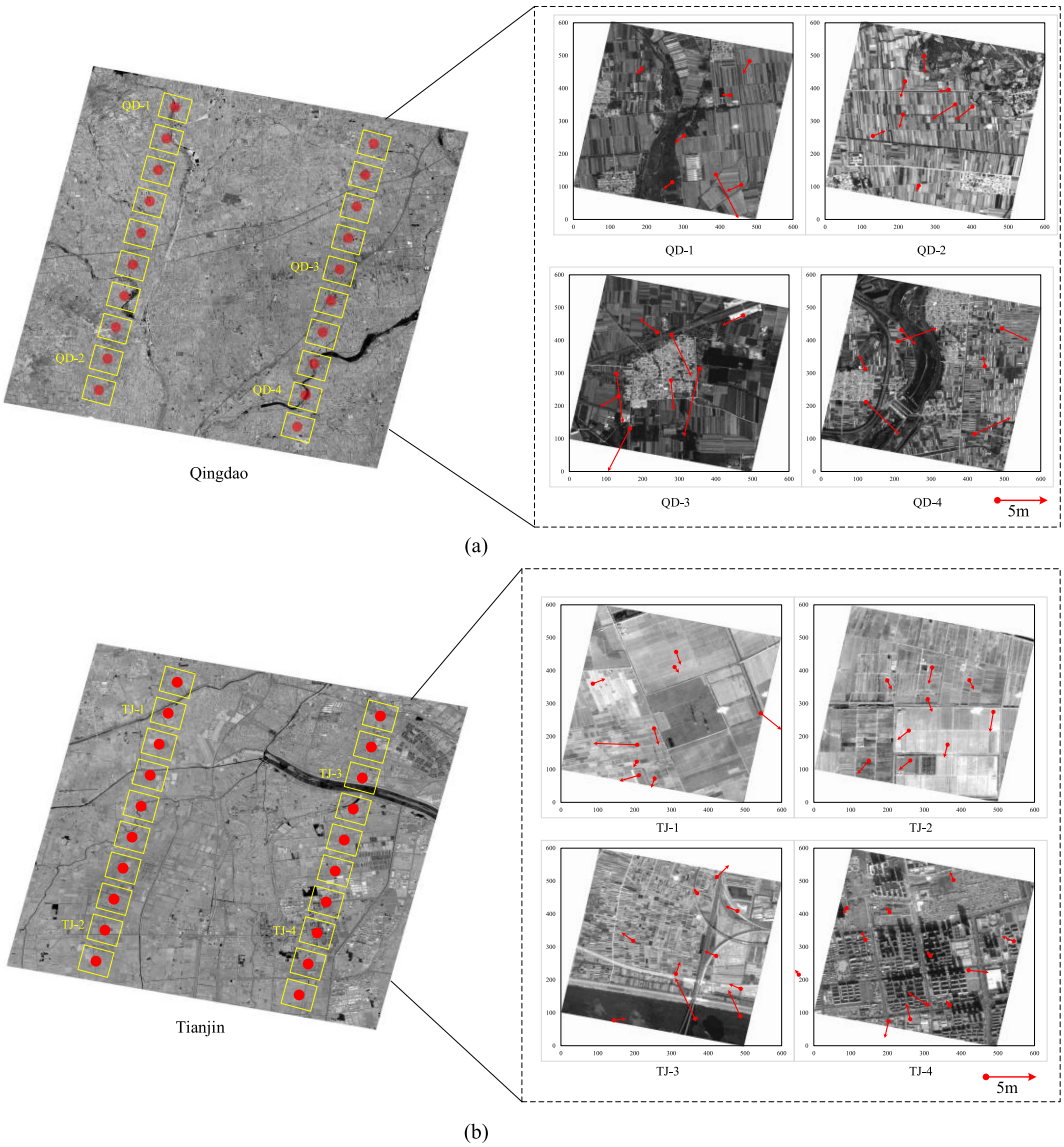

Fig. 13. Error distribution diagram of laser footprint images. (a) Qingdao experimental area. (b) Tianjin experimental area.

obtained within 4.0 m after the geometric calibration based on the simulation experiment. The errors of geometric calibration for the laser altimeter and footprint camera are independent of each other. Then, the following experiment is conducted to verify the relative positioning accuracy of the footprint camera to the dual-linear array cameras.

2) Verification of Positioning Accuracy: After determining the geometric relationship between the laser altimeter and the footprint camera, verification is focused on the positioning accuracy of the footprint images relative to the dual-linear array images. The validation experiment of cameras on the GF-7 satellite was performed in Qingdao and Tianjin, China. Four frames of footprint camera images in each of the two regions were verified for positioning accuracy using dual-linear array images as the reference standard. The relative positioning errors of the footprint images were determined by image matching, whereas the join points between the dual-linear array images and footprint images were used as checkpoints. The results of the experiment in the two study regions are listed in Table IV, and the error distributions for the relative positioning accuracy of the footprint images are shown in Fig. 13.

The experimental results show a positioning accuracy of 3.172 m for the footprint camera images relative to the dual-linear array images in Qingdao and a positioning accuracy of 3.326 m in Tianjin. It is shown that the average positioning accuracy of 3.25 m for the footprint camera images is relative to the dual-linear array images. There are some mismatch points that are deleted in the image matching. We can see that the maximum error and minimum error are less than three times the root-mean-square error (RMSE) in Table IV. According to the geometric positioning model of the laser altimeter, the positioning error of the laser spot relative to the dual-linear array image mainly includes two types of error: the calibration error of the laser altimeter and footprint camera, and the relative positioning error of the footprint camera

TABLE IV
POSITIONING ERRORS BETWEEN FOOTPRINT CAMERA AND DUAL-LINE CAMERA

Experimental area	Footprint image	Number of checkpoints	RMSE (m)			Maximum error (m)		Minimum error (m)	
			X	Y	XY	X	Y	X	Y
Qingdao	QD-1	7	1.326	1.711	2.164	1.612	3.529	–2.461	–1.905
	QD-2	9	1.247	1.671	2.085	2.545	0.309	–1.385	–3.855
	QD-3	9	1.861	4.335	4.717	2.512	7.567	–2.237	–3.592
	QD-4	8	2.686	2.576	3.722	0.676	2.132	–4.208	–3.825
Total		33	1.781	2.573	3.172	2.545	7.567	–4.208	–3.855
Tianjin	TJ-1	9	3.291	2.066	3.886	7.925	3.363	–3.741	–1.013
	TJ-2	9	1.348	2.653	2.976	2.090	4.091	–0.828	1.903
	TJ-3	11	2.075	3.248	3.854	3.602	–0.255	–2.205	–8.241
	TJ-4	11	1.781	1.875	2.586	3.601	3.375	–3.658	–3.161
Total		40	2.124	2.461	3.326	7.925	4.091	–3.741	–8.241

and dual-linear array camera. These two types of errors are independent of each other. So, the relative positioning accuracy of the laser spots can be determined according to the theory of measuring errors. Considering the laser calibration, platform stability, and data processing errors, the RMSE of the laser spots can reach approximately 5.0 m relative to the dual-line array images. The laser altimeter of the GF-7 satellite can provide elevation control data for high-resolution stereo mapping in areas lacking GCPs.

V. CONCLUSION

In this study, the error transmission and accuracy of the measurement link between the laser altimeter and footprint camera of the GF-7 satellite were analyzed, and an RSM of the satellite laser altimeter was constructed based on the coupled footprint camera. Validation experiments were conducted using simulated data and GF-7 satellite data, and the following conclusions were obtained based on the experimental results.

1) The error source for laser spot positioning is analyzed in the simulation experiment, including the satellite platform and geometric calibration. The accuracy of GCPs from ground detectors is limited due to the detector interval and the consistency ratio. The accuracy error of the laser spot's center on the footprint images can achieve 0.3 pixels using the improved algorithm in this study.
2) The positioning accuracy of the footprint camera on the GF-7 satellite is better than 5.0 m relative to the dual-line array cameras, and it can provide elevation control data for stereo mapping in areas lacking GCPs.

REFERENCES

[1] A. Donges and R. Noll, *Laser Measurement Technology: Fundamentals and Applications*. Berlin, Germany: Springer, Jun. 2015, pp. 4–20.
[2] X. Tang and G. Li, *Earth Observation Satellite Laser Altimetry Data Processing and Project Practice*. Beijing, China: Chin. Sci. Press, Mar. 2019, pp. 34–44.
[3] J. B. Abshire et al., "Geoscience laser altimeter system (GLAS) on the ICESat mission: On-orbit measurement performance," *Geophys. Res. Lett.*, vol. 32, Nov. 2005, Art. no. L21S02.
[4] B. E. Schutz, H. J. Zwally, C. A. Shuman, D. Hancock, and J. P. DiMarzio, "Overview of the ICESat mission," *Geophys. Res. Lett.*, vol. 32, no. L21S01, pp. 97–116, Nov. 2005.
[5] X. Wang, X. Cheng, P. Gong, H. Huang, Z. Li, and X. Li, "Earth science applications of ICESat/GLAS: A review," *Int. J. Remote Sens.*, vol. 32, pp. 8837–8864, Aug. 2011.
[6] M. Hayashi, N. Saigusa, H. Oguma, and Y. Yamagata, "Forest canopy height estimation using ICESat/GLAS data and error factor analysis in Hokkaido, Japan," *ISPRS J. Photogrammetry Remote Sens.*, vol. 81, no. 7, pp. 12–18, Jul. 2013.
[7] K. M. Brunt, T. A. Neumann, and C. F. Larsen, "Assessment of altimetry using ground-based GPS data from the 88S Traverse, Antarctica, in support of ICESat-2," *Cryosphere*, vol. 13, pp. 579–590, Mar. 2019.
[8] D. Gwenzi, M. A. Lefsky, V. P. Suchdeo, and D. J. Harding, "Prospects of the ICESat-2 laser altimetry mission for savanna ecosystem structural studies based on airborne simulation data," *ISPRS J. Photogrammetry Remote Sens.*, vol. 118, no. 8, pp. 68–82, Aug. 2016.
[9] D. B. Coyle, P. R. Stysley, D. Poulios, G. B. Clarke, and R. B. Kay, "Laser transmitter development for NASA's global ecosystem dynamics investigation (GEDI) lidar," *Proc. SPIE*, vol. 9612, Sep. 2015, Art. no. 961208.
[10] P. R. Stysley et al., "Laser production for NASA's global ecosystem dynamics investigation (GEDI) lidar," *Proc. SPIE*, vol. 9832, May 2016, Art. no. 983207.
[11] D. Li, Q. Tong, R. Li, J. Gong, and L. Zhang, "Current issues in high-resolution earth observation technology," *Sci. China Earth Sci.*, vol. 55, pp. 1043–1051, Jun. 2012.
[12] R. Wang and J. Wang, "Technology of bundle adjustment using two-line-array CCD satellite image combined laser ranging data," *J. Geomatics Sci. Technol.*, vol. 31, pp. 1–4, Jan. 2014.
[13] G. Li and X. Tang, "Analysis and validation of ZY-3 02 satellite laser altimetry data," *Acta Geodaetica Cartographica Sin.*, vol. 46, no. 12, pp. 1939–1949, Dec. 2017.
[14] J. Xie et al., "ZY3-02 laser altimeter footprint geolocation prediction," *Sensors*, vol. 17, no. 10, Sep. 2017, Art. no. 2165.
[15] X. Tang, C. Liu, and Z. Heng, "GF-7 satellite stereo images block adjustment assisted with laser altimetry data," *Geomatics Inf. Sci. Wuhan Univ.*, vol. 42, pp. 1423–1430, Oct. 2021.
[16] G. Zhang, S. Li, C. Huang, and D. Li, "Geometric calibration and validation of ZY3-02 satellite laser altimeter system," *Geomatics Inf. Sci. Wuhan Univ.*, vol. 42, no. 11, pp. 1589–1596, Nov. 2017.

[17] X. Tang, J. Xie, X. Gao, F. Mo, W. Feng, and R. Liu, "The in-orbit calibration method based on terrain matching with pyramid-search for the spaceborne laser altimeter," *IEEE J. Sel. Topics Appl. Earth Observ. Remote Sens.*, vol. 12, no. 3, pp. 1053–1062, Mar. 2019.
[18] P. Zhou, X. Tang, D. Li, and X. Wang, "Combined block adjustment of stereo imagery and laser altimetry points of the ZY3-03 satellite," *IEEE Geosci. Remote Sens. Lett.*, vol. 19, 2022, Art. no. 6506705.
[19] H. Cao, X. Zhang, C. Zhao, C. Xu, F. Mo, and J. Dai, "System design and key technologies of the GF-7 satellite," *Chin. Space Sci. Technol.*, vol. 40, no. 5, pp. 1–9, May 2020.
[20] G. Li et al., "Processing and preliminary accuracy validation of the GF-7 satellite laser altimetry data," *Acta Geodaetica Cartographica Sin.*, vol. 50, no. 10, pp. 1338–1348, Oct. 2021.
[21] G. Huang, Y. Ding, J. Wu, R. Shu, X. Wang, and Z. Jiang, "Design and implementation of key technology of GF-7 satellite laser altimeter subsystem," *Spacecraft Eng.*, vol. 29, no. 3, pp. 68–73, Mar. 2020.
[22] J. Xie et al., "Design and data processing of China's first spaceborne laser altimeter system for earth observation: GaoFen-7," *IEEE J. Sel. Topics Appl. Earth Observ. Remote Sens.*, vol. 13, pp. 1034–1044, 2020.
[23] X. Tang et al., "GF-7 dual-beam laser altimeter on-orbit geometric calibration and test verification," *Acta Geodaetica Cartographica Sin.*, vol. 50, no. 3, pp. 384–395, Mar. 2021.
[24] H. Xie et al., "A planimetric location method for laser footprints of the Chinese Gaofen-7 satellite using laser spot center detection and image matching to stereo image product," *IEEE Trans. Geosci. Remote Sens.*, vol. 59, no. 11, pp. 9758–9771, Nov. 2021.
[25] J. Xie, C. Ren, H. Jiao, and J. Pan, "In-orbit geometric calibration approach and positioning accuracy analysis for the Gaofen-7 laser footprint camera," *IET Image Process.*, vol. 15, no. 13, pp. 3130–3141, Nov. 2021.
[26] J. Yao, G. Li, J. Chen, G. Huang, X. Yang, and S. Zhang, "Cloud detection and centroid extraction of laser footprint image of GF-7 satellite laser altimetry," *J. Geodesy Geoinf. Sci.*, vol. 4, no. 3, pp. 1–12, Mar. 2021.
[27] Y. Jiang et al., "CCD distortion calibration without accurate ground control data for pushbroom satellites," *ISPRS J. Photogrammetry Remote Sens.*, vol. 142, pp. 21–26, Aug. 2018.
[28] H. Pan, T. Huang, and Z. Cui, "Self-calibration dense bundle adjustment of multi-view worldview-3 basic images," *ISPRS J. Photogrammetry Remote Sens.*, vol. 176, pp. 127–138, Jun. 2021.

Shaoning Li was born in June 1985. He received the Ph.D. degree in photogrammetry and remote sensing from the State Key Laboratory of Information Engineering in Surveying, Mapping and Remote Sensing, Wuhan University, Wuhan, China, in 2017.

Since 2017, he has been a Postdoctoral Researcher with Wuhan University. Since 2020, he has been with the National-Local Joint Engineering Laboratory of Geo-Spatial Information Technology, Hunan University of Science and Technology, Xiangtan, China, where he became an Associate Professor in 2021. His research interests include the processing and applications of satellite laser altimeters.

Guo Zhang (Member, IEEE) received the B.E. and Ph.D. degrees in photogrammetry and remote sensing from the School of Remote Sensing and Information Engineering, Wuhan University, Wuhan, China, in 2000 and 2005, respectively.

His Ph.D. dissertation was on the rectification of high-resolution remote sensing images with a lack of ground control points. Since 2005, he has been with the State Key Laboratory of Information Engineering in Surveying, Mapping, and Remote Sensing, Wuhan University, where he became a Professor in 2011. His research interests include space photogrammetry, including the processing and applications for optical load, synthetic aperture radar load, video load, and laser load.

Xiufang Fan was born in December 1997. She is currently working toward the M.S. degree in resources and environment at the School of Earth Science and Spatial Information Engineering, Hunan University of Science and Technology (HNUST), Xiangtan, China.

She has been with the National-Local Joint Engineering Laboratory of Geo-Spatial Information Technology, HNUST, since 2020. Her research interests are mainly focused on satellite-based LiDAR data processing.